



EVALUATION OF TUFF CELLAR STABILITY BY APPLYING THE CONVERGENCE-CONFINEMENT METHOD

POSÚDENIE STABILITY TUFOVÝCH PIVNÍC DEFORMAČNOU METÓDOU

Pavol Vavrek¹, Edita Lazarová², Mária Bali Hudáková³, Alexander Kiovský⁴, Vít'azoslav Krúpa⁵, Lucia Ivaničová⁶

Abstract

Stability of underground structures is typically assessed by applying various mathematical modelling methods (FEM, FDM, DEM). One of the options is to apply the Convergence-Confinement Method (CCM), which was primarily used in the period when the modern tunnel industry was emerging. In this paper, the identified graphical curves of the deformation characteristics of a rock massif (In Slovak)-Ground Reaction Curve (GRC) and the deformation characteristics of the support (In Slovak) – Support Characteristic Curve (SCC) were used to identify the load to which the support was exposed, as well as the deformation of the excavated part of the underground structure and safety of the rock-support system. This article presents a description and practical application of CCM with regard to tuff cellars.

Abstrakt

Posudzovanie stability podzemných diel sa v súčasnosti realizuje hlavne pomocou rôznych metód matematického modelovania (Metóda konečných prvkov - FEM, Metóda konečných diferencií - FDM, Metóda oddelených prvkov - DEM). Jednou z alternatív, ktorá sa dá použiť je aplikácia deformačnej metódy, ktorá bola využívaná hlavne v období nástupu moderného tunelárstva. Zo známeho grafického priebehu deformačnej charakteristiky horninového masívu a deformačnej charakteristiky výstuže sa stanoví veľkosť zaťaženia výstuže, deformácia výlomu podzemného diela a stupeň bezpečnosti systému hornina - výstuž. Príspevok sa zameria na popis a praktickú aplikáciu deformačnej metódy na podmienky tufových pivníc.

Keywords

Stability, convergence -confinement method, ground reaction curve, support characteristic curve, tuff cellars

Klíčové slová

Stabilita, deformačná metóda, deformačná charakteristika masívu, deformačná charakteristika výstuže, tufové pivnice

1. Introduction

Underground structures have been used by the mankind since the ancient times. They were first simply used as underground spaces (caves), later adjusted to secured, and eventually used by the mankind for building artificial underground objects for various purposes (religious, defence, water management, communication, etc.) (Ratkovský, K. ; Klepsatel, F., 1980).

Multiple underground structures can be found, dating back to the ancient times. The first water tunnels were built as oval 'qanats' to serve towns, especially in Mesopotamia and Iran. Those structures were built since 3rd millennium BC, primarily in soils (Girmscheid, G., 2008; Klepsatel, F. et al., 2005).

In ancient Babylon, approximately 2,500 years BC, the Queen Semiramis ordered the construction of an underground corridor connecting her palace with the temple under the Euphrates River. The tunnel that was approximately 900 m long was built in an open trench while the Euphrates River was temporarily relocated to flow through a bypass channel (Ratkovský, K., Klepsatel, F., 1980; Girmscheid, G., 2008).

Probably the oldest underground structure is a cult complex – Hypogeum in Hal Safiens, near the town of La Valetta on the Malta island. It was built in the period after year 2400 BC (Klepsatel, F. et al., 2005).

The first water tunnel, excavated in rock, was located in the oldest part of the aqueduct in Jerusalem; it was built in the times of King Solomon (Klepsatel, F. et al., 2005).

One of the most interesting ancient structures is a drainage tunnel built in the times of Caesar in years 50–46 BC, which was used for draining water from the Fucine Lake; it was approximately 5,600 m long and its clear cross-sectional area was 1.8 x 3.0 m (Klepsatel, F. et al., 2005).

One of the first recognised road tunnels is the tunnel near Cumae between Napoli and Pozzuoli, 690 m long, built by the Roman emperor Octavian (Ratkovský, K., Klepsatel, F., 1980; Girmscheid, G., 2008; Klepsatel, F. et al., 2005).

After the fall of the Roman Empire in the Middle Ages, the construction of underground structures was in recess. Underground works were limited to the construction of military structures (emergency exit corridors from buildings, monasteries, etc.). A new impulse for the development of the underground building industry was the development of the mining industry, primarily the underground excavation of precious metals.

The Modern Era is mainly associated with the construction of traffic structures, such as ship tunnels that were built in 17th–19th century, followed by the construction of railway tunnels, and later on also road tunnels.

In addition to the underground structures for traffic, water management, power and defence purposes, there is also a category of other underground structures, the importance of which is currently increasing. Those underground structures include sporting centres, museums, galleries, waste water plants etc.

Traditionally, other underground structures were mostly wine cellars. They were built where conditions were suitable for growing wine grape, i.e. primarily in the Mediterranean. Expansion of the viticulture may be attributed to ancient Greeks and Romans, who shifted the borders of viticulture regions to Central Europe and Rhineland (Klepsatel, F. et al., 2005).

Extensive wine cellars can also be found in the Tokaj Wine Region, which is a geographically enclosed region of viticulture and viniculture in the Bodrog River basin, surrounded on its north side by the Zemplínske Mountains and the Rozhľadňa Hill (469 m a. s. l.) in Slovakia and on its south side by the confluence of the Tisa and Bodrog Rivers in Hungary (Fig. 1). It is a historical and territorial part of the Tokaj Region, a major part of which is located in Hungary (ca 5,000 ha). In Slovakia, its surface area defined by law is 907 ha. It is the smallest viticultural area in Slovakia.

Wine cellars are being built in that region even today. They may be located in less suitable geological and geotechnical conditions and exposed to additional surface load induced by, for example, new investment structures built above the existing underground spaces where the overburden layer is thin. In such cases, assessment or evaluation of stability of such underground structures is required.



Fig. 1 Tokaj Region (Geoslovakia, 2010)



Fig. 2 Area of interest – Velká Bara (Geoslovakia, 2010)

Early in the 21st century, an investor decided to build a wine-making complex, comprised of above-ground and underground premises, at the south-west border of Velká Bara village on the southern slope of the Piliš Hill (Fig. 2).

2. Engineering and geological conditions at the Veľká Bara location

Based on the geomorphology of Slovakia, the area of interest is part of the Matra-Slanec Area in the Zemplínske Mountains (Mazúr, E., Lukniš, M., 1986). A substantial part of the investigated area emerges on the south-west border of the Zemplínske Mountains.

The geological composition of the area of interest mostly consists of rocks that date back to the young Palaeozoic Era (Carboniferous and Permian), emerging in the Zemplínske mountains near Veľká Bara and Černochovej villages. They comprise layers located around Trňany, Kašov, Cejkov and Černochovej villages, characterised by rhyolite and dacite vulcanites, polymictic conglomerates, sandstones, shale and shaly claystones. Neogene vulcanites are the products of andesite and acid rhyolite vulcanism. They are characterised by lava flows of basaltoid andesites and their breaks, unsorted rhyodacite pumice tuffs and fine-grained redeposited rhyodacite tuffs. Quaternary sediments emerge mostly in the form of Holocene fluvial clays, proluvial clays and clay gravel, as well as unsegmented clay and clay-stone diluvial sediments (Baňacký, J. et al., 1986).

2.1 Exploratory engineering geological survey

In the exploratory stage of the engineering geological survey conducted in 2010, three core-drilled boreholes VBJ-1 to VBJ-3 were made to a depth of 15 m under the surface.

The identified engineering geological parameters of the collected lithology types were as follows:

- **A humus layer** with a thickness of 0.2–0.3 m;
- **Diluvial sediments** (CI and CV classes) collected at depths from 0.2–0.3 m to 0.9–2.1 m;
- The base of the investigated profile consisted of **significantly weathered and disrupted eluvium** formed of clay sand (CS) at a depth of 1.1–4.1 m under the surface;
- At a depth from 2.1–6.2 m under the surface to the final depth of 15 m, weathered eluvium of R6 class was found, represented by redeposited rhyodacite and tuffite breaks with primarily a clay-sand filling (Geoslovakia, 2010).

The presence of underground water was not observed in any of the VBJ-1 to VBJ-3 boreholes. With regard to the construction of underground cellars, the executor of the exploratory survey stated that “the geological conditions identified in the area of the planned construction site appear to be unsuitable for building cellars with natural arches. Based on the borehole drilling, no high-quality tuffs capable of transferring the load exerted from the surface through arches were found”.

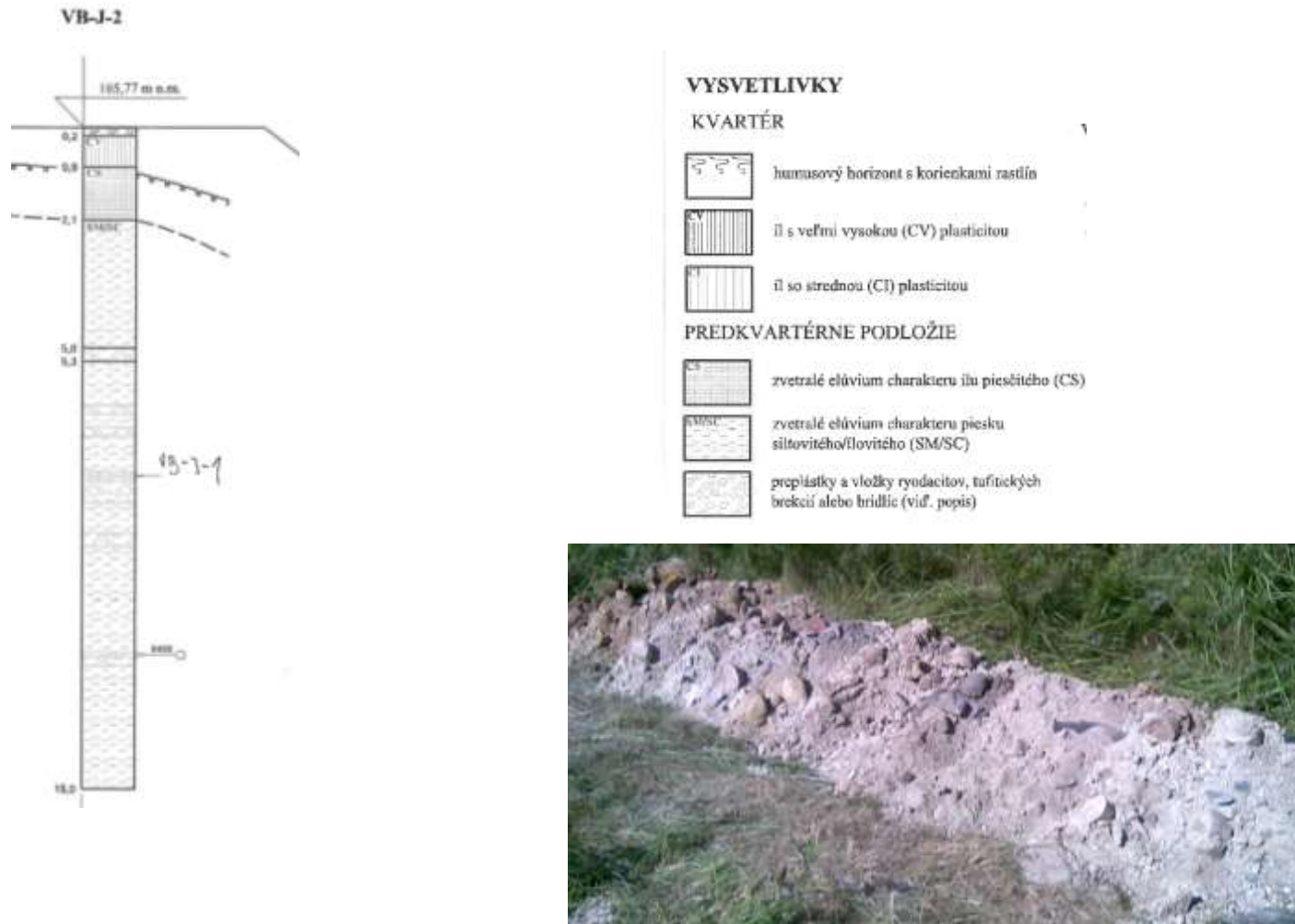


Fig. 3 Geological profile and photo documentation of the VBJ-2 borehole (Geoslovakia, 2010)

2.2 Additional engineering geological survey

In 2012, an additional engineering geological survey was conducted by MontanA, s. r. o. with the aim of verifying the presence of hard tuff massifs suitable for the construction of wine cellars. The survey zone was located further north of VBJ-1 to VBJ-3 boreholes. In that stage, 9 boreholes were drilled –VB1 to VB9. The composition of the layers of the individual cores was similar to that of the cores obtained in the exploratory survey. The top parts included humus layers of various thicknesses, mostly formed of dark brown soil. Below

them, there were layers of tuffite clays and clay sand of brown and light brown colour, 4 m thick. The bottom parts mostly included medium-grained grey-white and white tuffites with higher contents of pumice, containing also pieces of andesite (MontanA, 2012).



Fig. 4 Photo documentation of the VB-7 cores

Photo documentation of the VB-7 cores, showing the contour of the planned wine cellar (yellow) is presented in Fig. 4. In this stage of the survey, no underground water was detected at the depth drilled.

Even though the survey did not confirm the presence of tuffs with a strength sufficient for smooth digging of cellars, the investor nevertheless decided to construct underground structures in tuffite sands with a high degree of consolidation.

3. Geotechnical properties of tuffites and tuffs

As for the stability of tuff cellars in the Veľká Bara location, the most important rock materials are tuffites or tuffite sands, in which the underground structures have been excavated.

The eluvium is mostly formed of rhyolite or andesite redeposited volcanic and clastic layers in the form of tuffites (a pyroclastic sediment containing mixed volcanic and terrigenous materials). In the region where the wine cellars have been built, the dominating sediment is fine-grained and pyroclastic (tuffite sand).

In the engineering geological survey (EGS) of the Veľká Bara location, the following geological works were carried out:

Exploratory engineering geological survey (Geoslovakia, s.r.o.) – 2010,

Exploratory engineering geological survey (MontanA, s.r.o.) – 2012,

Additional engineering geological survey (MontanA, s.r.o.) – 2012.

Results of the individual stages of the exploratory engineering geological survey did not provide the necessary geotechnical (shear) parameters of tuffite sands. In the additional engineering geological survey, additional parameters of rocks were identified (uniaxial compressive strength); however, since the test samples did not have the required dimensions and their preparation was difficult, their explanatory power was not sufficient.

3.1 Physical and mechanical properties of tuffites and tuffite sands

In May 2022, an engineering geological survey was conducted near the Velká Bara Winery with the aim of assessing the possibilities of building tuff cellars there. The survey included laboratory research aimed at identifying shear strength of tuffite clays and tuffites found in the Velká Bara location, in particular on the southern slope of the Piliš Hill, which were not examined in years 2010–2012.

Shear strength

Shear parameters of soils (c – cohesion, ϕ – angle of friction) were identified using a triaxial equipment, while one of the samples was tested using a shear box testing equipment (Fig. 5 and 6).

The first sample was tested in the shear box testing equipment. Due to certain difficulties in the preparation of test samples for that type of test (a sample diameter of 100 mm), the following samples were tested in the triaxial equipment while the diameter of the samples (cylinders) was 38 mm (Table 1).

The VBP-22 and 23 samples were taken from the consolidated positions of fine-grained sediments – tuffite sands. Triaxial tests were carried out as multi-level consolidated tests. For tuffite clays, the test outcomes were total shear parameters, while for light tuffite sands, the outcomes were shear effective parameters, similarly to the direct shear box test.

Fig. 7 and Fig. 8 show the curves of the monitored parameters (chamber pressure – kPa, axial force – N, axial displacement – mm) and the evaluation of the triaxial test with the VBP-23 sample.



Fig. 5 Triaxial equipment Fig. 6 Shear box testing equipment

Tab. 1 Parameters of test samples

Designation of samples	Collection site and depth	Test sample diameter d [mm]	Water content w [%]	Bulk density ρ_0 [kg.m ⁻³]
VBP-22	VBP-2, depth of 9.0–9.2 m	100	25.6	1,600
VBP-23	VBP-2, depth of 12.8–13.0 m	38	26.7	1,700

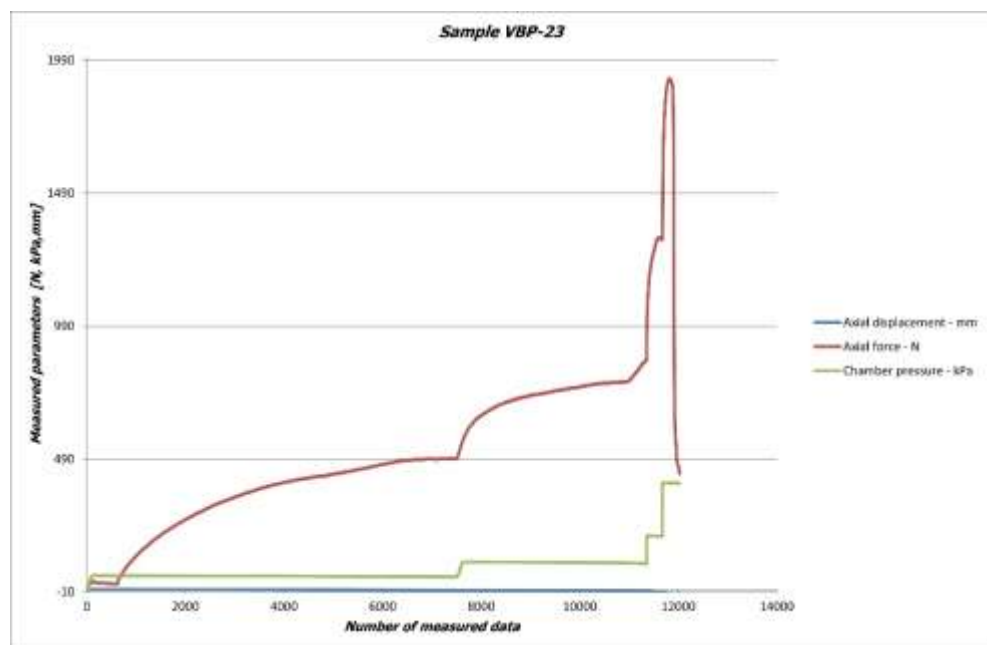


Fig. 7 Curves of the measured parameters

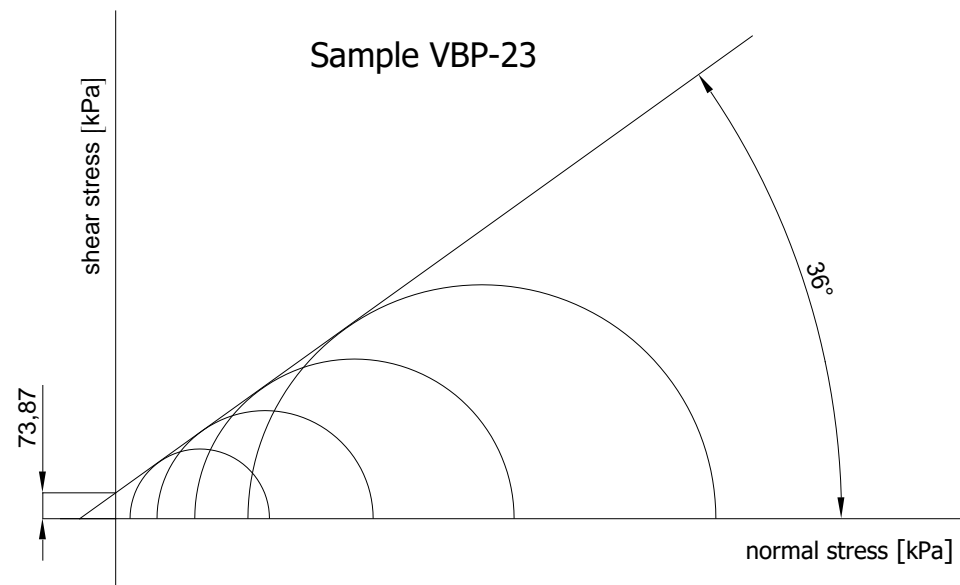


Fig. 8 Evaluation of the triaxial test

The summary table (Table 2) below contains the resulting values of shear strength. The parameters of relevant rock types stated above (Tables 1 and 2) were used to identify the parameters of the rock massif for the lithological type – tuffites.

Tab. 2 Shear strength of tuffites

Designation of samples	Collection site and depth	Shear strength	
		c_{ef} (kPa)	Φ_{ef} (°)
VBP-22	VBP-2, depth of 9.0–9.2 m	12	53
VBP-23	VBP-2, depth of 12.8–13.0 m	74	36

It should be noted that the properties shown in Table 2 are of the point laboratory nature and, therefore, must be adjusted to the analysed rock massif. Foreign literature specifies a wide range of geotechnical parameters of tuffites and tuffite sands (Table 3).

Tab. 3 Properties of tuffite sands

Sources Lithological type	Bulk density ρ_o [kg.m ⁻³]	Modulus of elasticity E [MPa]	Poisson's ratio μ [-]	Angle of friction ϕ [°]	Cohesion c [kPa]
<i>Contreras, C., A., et al., 2010</i> <i>Tuff sand, Breccias</i>	2,500	2,484	0.3	38	210
<i>Santolo, A. S., et al., 2015</i> <i>Pozzolana</i>	1,500	336	0.3	33	15
<i>Covassi, A. P., et al., 2015</i> <i>Pyroclastic sand</i>	1,250	-	-	39	7
<i>Asniar, N. et al., 2019</i> <i>Tuff soil</i>	1,000–2,600	-	-	10–40	7–100
<i>Vavrek, P., 2022</i> <i>Tuffite sand</i>	1,600–1,700	-	-	36–53	12–74

One of the most complex publications providing a review of the properties of tuffite soils and tuffs is the one published by Asniar, N. et al. (2019). According to that review, cohesion of tuffites ranges from 0.007 to 0.1 MPa. Cohesion of saturated tuffites amounts to 0.032 MPa. The angle of friction ranges from 10° to 40°. For the purpose of assessing stability of the tuff cellars, the tuffite zones were assessed based on the following values of shear strength: $coh = 30$ kPa (according to Asniar, N. et al., 2019) and $fri = 36^\circ$ (according to Vavrek, P., 2022).

According to the opinion of the authors of the article, construction of a surface structure on a land that has been partially excavated underground and comprises a shallow overburden layer falls within the Geotechnical Category 3. A survey for the Geotechnical Category 3

must provide characteristics of the underlying soils; those were identified based on the results of the tests conducted directly on the construction site. In the survey, samples collected had to be both disturbed and disturbed for the purpose of laboratory investigation customised to a particular survey project; alternatively, in-field tests should be carried out. Since the local characteristics of soils, identified based on the results of the tests conducted in the survey on the construction site, were not available, analytical calculations were made using the properties described in literature published by foreign authors (Asniar, N. et al., 2019) as well as local characteristics (Vavrek, P., 2022).

According to a paper (Barták, J. et al., 2010) based on Eurocode 7, geotechnical parameters were calculated using respective partial coefficients of the properties of rocks or soils γ_{kr} for the ultimate limit state. However, the above-mentioned paper did not specify partial coefficients for mean values of deformation parameters (modulus of elasticity, modulus of deformation), only the Poisson's ratio was specified; therefore, their values were used without making adjustments with the use of those partial coefficients.

3.2 Physical and mechanical properties of tuffs - facing stone

In terms of stability of the wine cellars, important parameters also included the properties of tuffs that were used as a permanent support in the form of a cladding made of facing stones installed using cement mortar.

The support was built using quarry tuff stones taken from the Kerestúr location (Hungary). The quarry stones were subjected to testing in 2012/2013 and in 2025 with the aim of identifying their basic physical and mechanical properties, which had to be identified in order to assess stability of the permanent support and its surroundings. The test samples were drilled out of the pieces of tuff rock specimens and further trimmed to obtain the required dimensions. Subsequently, the samples were subjected to strength testing following the ISRM requirements (Fig. 9). The summary results are presented in Table 4.

Tab. 4 Properties of tuffs

Test year	Properties					
	ρ_o [kg.m ⁻³]	σ_{ct} [MPa]	σ_{tt} [MPa]	σ_{ft} [MPa]	E_{tl} [MPa]	μ_t [-]
2012/2013	1,414	9.3	1.7	-	840	-
2025 – dry state	1,380	5.8	0.9	1.8	1,500	0.4
2025 – wet state	1,650	4.7	0.8	1.4	1,208	0.43

Legend: ρ_o – bulk density, σ_{ct} – uniaxial compressive strength, σ_{tt} – transverse tensile strength, σ_{ft} – flexural (bending) strength, E_{tl} – modulus of elasticity, μ_t – Poisson's ratio.

Around the turn of 2012 and beginning of 2013, the test samples were tested at a water content corresponding to laboratory conditions. In 2025, strength tests were carried out in the dry state (in laboratory conditions) at a water content (w) of 0.6 % in the test samples, and in the wet state.

The tuff test samples were tested for absorption rate; subsequently, their strength and deformation properties were identified after being saturated with water. The absorption rate was identified as 48 hours in a test consisting of gradual pouring of water onto the test samples. During the strength tests, the water content $w = 21.6\%$. The water content of the tuff stone in situ was 22.4% (piece samples were collected underground, put into a plastic bag and taken to the laboratory for testing with the aim of identifying their water content).

The identified properties of tuff stones after being saturated with water were comparable to the properties of the tuff facing stones used as the permanent support in the underground cellars (Fig. 10), which was also proven by the water content values specified above ($w = 21.6\%$ in strength testing and $w = 22.4\%$ in the tuff stones located underground in situ).

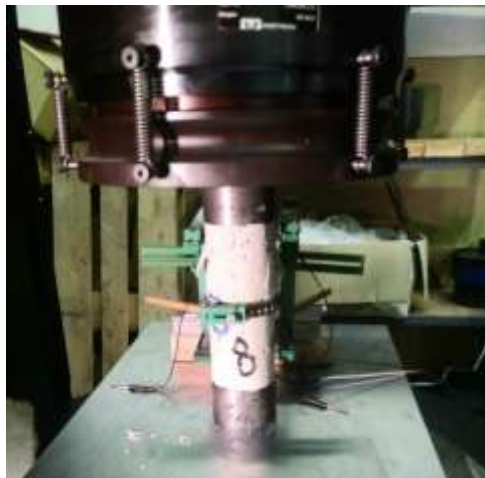


Fig. 9 Testing of deformation properties Fig. 10 Arch support with variable thickness

Fig. 11 Schmidt Hammer

Similarly to the tuffite parameters, the load-bearing capacity of the permanent tuff support is one of the crucial characteristics that affect stability of the underground premises; they should transfer additional loads exerted, for example, by newly-built surface structures above the tuff cellars.

It should be kept in mind that the permanent support is a cladded structure (tuff blocks were attached to cement mortar or cement seal). The tuff support was built using adhesive mortar (glue) mixed with sieved tuffite sand as a binder.

The Schmidt Hammer test was conducted at two different underground locations to examine the strength of the cement seal and of the tuff blocks. The tests were carried out in the direction perpendicular to the test surface. At each test location, ten measurements were carried out on the tuff stones and cement seal. The in-situ measurements were carried out using a type N Hammer (Fig. 11) with an energy of 2.25 J.

Average rebound values R , as identified at two measurement sites on the tuff stones, were $R = 24$ and $R = 25$. As for the cement mortar, the rebound values were $R = 23$ and $R = 20$.

Based on a comparison of the average strengths of tuff and of mortar, as identified in the Schmidt test, it may be stated that the sealing mortar exhibited strength 12 % lower than that of tuff.

4. Convergence-Confinement Method

One of the key tasks that are required in any underground activities, including underground mining of minerals and building underground engineering structures, is to ensure stability of underground premises. Successful execution of practical tasks related to rock mechanics is conditioned by understanding mechanical characteristics of relevant rock massifs. The efforts aimed at defining, as accurately as possible, mechanical characteristics of rocks are accompanied by the development of theories and methods regarding stability of underground mining spaces. Contemporary engineering activities are typically characterised by efforts aimed at optimising every construction and developing a solution that is not only technically perfect, but also cost-efficient. In technical practice, various methods of executing geotechnical tasks are currently applied. They are categorised into three basic groups:

- Analytical methods;
- Experimental methods; and
- Numerical methods.

One of the most frequently used analytical methods used in the process of designing supports for mining and underground engineering linear structures and assessing their stability is the *Convergence-Confinement Method (CCM)* developed by Pacher (1964). It has become the basic analytical tool for the New Austrian Tunnelling Method, originally developed by Fenner (Fenner, R.,1938). The Fenner's solution did not take into consider cohesion in ideal elastic-plastic behaviour of a rock environment. That approach was later improved by Salencon,J. (1969) and further extended by Kastner,H. (1971); Kabwe, E. et al., 2020.

Over the last 30 years, many authors (Brady,B.G.H.,Brown,E.T.,1985; Carranza-Torres, C.,2003; Duncam Fama, M.E.,1993; Hoek, E., 1990,1998,1999; Hoek, E., Brown, E. T.,1980,1997; Lee,Y.K., Pietruszczak, S., 2014; Oreste,P.P, Peila, D.,1997; Panet, M., Guenot, A., 1983; Panet, M., 1995; Vlachopoulos, N., Diederichs, M.S., 2009 etc.) have studied, developed, and promoted CCM as the method to be used in geotechnical practice.

The process of ensuring stability of linear underground structures by applying the CCM is based on identifying the following:

- Deformation characteristics of the massif (Ground Reaction Curve),
- Deformation characteristics of the support (Support Characteristic Curve), and
- Deformation profile in the longitudinal axis of the excavated structure (Longitudinal Deformation Profile).

The CCM is currently regarded as one of the most ideal theoretical methods for explaining the interactions between the excavated part of an underground structure and the surrounding rock in terms of stress and strain.

Identifying behaviour of stresses around an underground structure is only the first step in the process of ensuring stability of horizontal mining workings or underground engineering structures. It should be kept in mind that every change in the stresses is accompanied by corresponding deformation. Based on the support reaction pressure and type, two different states may occur:

- at $p_i \geq p_{cr}$ – the state of total stability
- at $p_i \leq p_{cr}$ – the state of partial stability

wherein p_i is reaction of the support on the walls of the tunnel (cellar); p_{cr} – the critical value of the support's reaction; u_{cr} – radial deformation in the form of displacement of the excavation boundary at the critical value of the support reaction.

At subcritical depths, i.e. where the concentration of stresses on the excavation boundary does not reach critical values in terms of rock strength and where a zone of inelastic deformations is not formed behind the excavation boundary, the correlation between the rock displacement on the excavation boundary and the support reaction pressure is linear. At $p_i \leq p_{cr}$ behind the excavation boundary, a zone of plastic deformations with an external radius R_p is formed. Deformation characteristics of the massif for the state of partial stability are non-linear; at $p_i = 0$, deformations of the excavated part of the underground structure without a support become terminal – maximum radial displacement u_r^{\max} (Fig. 12). In the case that an underground structure is excavated in mostly poor rock mass, a zone is formed where the material loosens and rocks eventually fall out. Such structures are therefore unstable without a support. In such a case, deformation characteristics of the massif in the zone of plastic behaviour are convex.

4.2 Deformation characteristics of the support (SCC)

Resistance pressure of the support is only manifested when it is deformed due to the displacement of the excavated part u_r and the gravitational force exerted by broken rocks in the ceiling of the excavated part. The correlation between the support resistance pressure p_i and the support displacement u_r , or between the support deformation and the load exerted on the support, $u_r = f(p_i)$, is referred to as the deformation characteristics of the support of an underground structure. Deformation characteristics of the support is a parameter that is a function of deformation properties of the support's material and thickness.

A support in an underground structure is concurrently affected by at least two elements with different deformation characteristics. Deformation of the support is accompanied not only by a decrease in the clear cross-sectional area of the underground structure, but also by an increase in the radial resistance pressure of the support; this means that the support increases stability of the process of deformation of the rock shell around it.

An important value that is part of the deformation characteristics of the support is its terminal point, i.e. its maximum value p_s^{\max} – the maximum support capacity before failure, which depends on the strength of the support material and the support thickness. Behaviour of the massif-support complex is also affected by the stiffness of the in-built support k_s (Fig. 12), which describes the slope of the linear region of deformation characteristics of the support to the vertical plane.

An intersection of the massif's deformation characteristics (GRC) and the support's deformation characteristics (SCC) is achieved when the internal resistance pressure of the support and the displacement of the excavated part of the underground structure are balanced; such balance corresponds to the factor of safety of the rock-support system $FoS = 1$ (Fig. 12).

4.3 Deformation profile (LDP)

Issues regarding the prediction of radial displacement of the excavated part of an underground structure have been studied by multiple authors. One of the theories that are most frequently applied is the Paneta's calculation, under which the course of radial displacement in the longitudinal axis of an underground structure is calculated using the λ coefficient and a distance d to which the primary support is built from the working face of the excavated structure. The λ coefficient is determined by empirical constants m and α and the radius of the excavated underground structure R . Hoek (1999) used the empirical equation for calculating a longitudinal deformation profile of an underground structure, which is a function of its radius, the maximum value of radial displacement of the excavated part at zero resistance pressure of the support, and the distance between the place where the support is built and the working face.

4.4 Assumptions of solution

Stability of an underground structure, when assessed by applying the CCM, is determined by the following conditions:

- A circular cross-section of the excavated structure with the tunnel of radius R ,
- A hydrostatic stress field σ_0 , which is a function of the depth of the structure excavated under the surface H and the bulk density of the overburden rocks ρ_0 ,
- Homogenous material properties of the rock mass, and
- Plane strain conditions.

However, the assumptions stated above are not realistic, and many authors (Feder,G., Arwatinakis, M., 1977; Kabwe,E. et al.,2020; Liu,N. et al., 2020; Vlachopoulos,N., Diederichs, M.S.,2014 etc.) have therefore tried to modify the CCM so that the analytical solution is as close as possible to the real conditions (a non-circular cross-section, an uneven stress field).

5. Assessment of stability of the tuff cellars by applying the CCM

A fundamental assessment of stability of the complex of tuff cellars was carried out through numerical geotechnical modelling of a continuum based on finite-difference methods in a 3D variant. Factors of safety (FoS) of the individual zones, calculated using the Mohr-Coulomb failure criterion for the variant without any load exerted on the terrain surface by the residential complex, acquired values $FoS \approx <1-1.2>$ at critical points of the model (immediate vicinity of the excavated structures in their ceilings and on their sides). When the load exerted on the terrain surface was taken into account, FoS values in the modelled zones decreased to $FoS = <0,8-1>$.

The validation of the numerical modelling results was carried out by applying an analytical method – the CCM, applied to the largest transverse cross-section existing underground, using a calculation parameter – a cross-section leading across the large testing room (Fig. 13, 16). The subchapters below provide brief results of the validation.

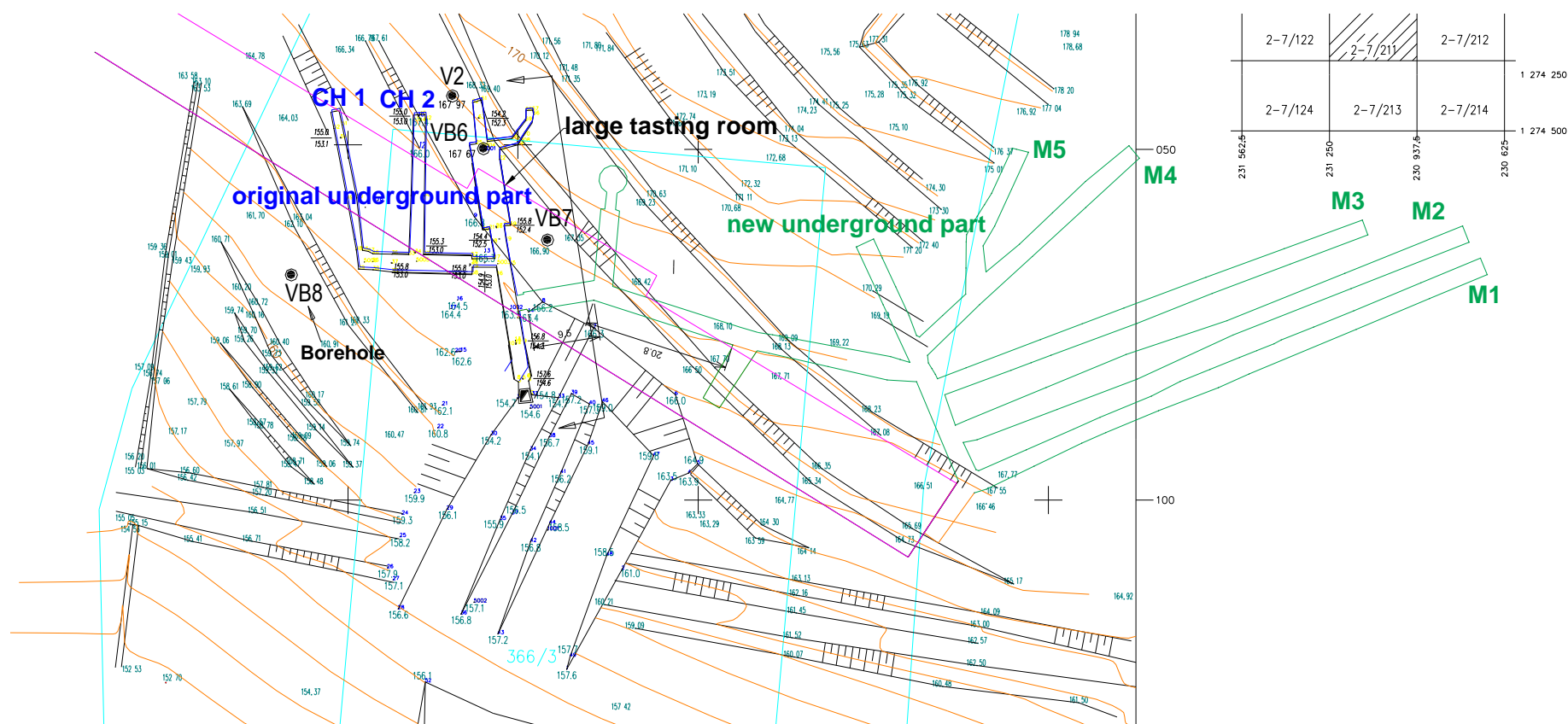


Fig. 13 Tuff cellars layout

The total length of the underground structures in the area in question was approximately 500 m. The original part of the underground premises (the layout of the underground structures shown in blue in Fig. 13) exhibited satisfactory results in terms of its stability. CH1 and CH2 corridors do not have any supports and they are currently used for wine ripening in barrels, while the other corridors (the winze, the archive corridor, and the large testing room) have tuff claddings. Unsupported corridors are horseshoe-shaped and their dimensions are approximately 2.2 x 2.2 m (w x h). The surface of the walls in the corridors was sufficiently moist and covered with a layer of humid materials and moulds; that prevents falling of materials from the walls and the arch (Fig. 14).



Fig. 14 CH1 mine – without a support Fig. 15 M2 corridor – a chimney shaft

The so-called “new section” of the underground premises (the contour of the underground structures in green and red, shown in Fig. 13 – the connecting and main corridors, the circular tasting room, and M1 to M5 corridors) were in a rather complicated state in terms of their stability. The structures with the tuff cladding were in good condition, while certain parts of the unsupported M1, M2, and M3 corridors were in bad condition as to their stability; they had chimney shafts shaped as vertical ellipses (Fig. 15) protruding up to the surface.

Therefore, the problematic sections of the corridors were filled with a cement-ashes mixture, while certain parts of the corridors were secured with a supporting steel frame with a OO-O-03 profile (an arch open in steel, size 03).

5.1 Deformation characteristics of the massif located in the large tasting room area (GRC)

The cross-section as a calculation parameter was based on the horseshoe cross-section of the large tasting room with a clear width of 4.4 m and a height of 3.85 m. The analysed structure has been excavated in tuffite sands with a bulk density $\rho_o = 1,650 \text{ kg.m}^{-3}$, while the higher overburden layer consisted of tuffite clays with a bulk density $\rho_o = 1,900 \text{ kg.m}^{-3}$ (Fig. 16).

Brown, Bray, Ladanyi and Hoek (1983) published equations that were used to calculate deformation characteristics of the massif in the area of the large tasting room while applying the Mohr-Coulomb failure criterion.

Average crack initiation stress σ_o [MPa] was calculated using equation (1) Carranza-Torres, Fairhurst (2000):

$$\sigma_o = \frac{\sigma_x + \sigma_z}{2} \quad (1)$$

where σ_x – horizontal stress [MPa], and
 σ_z – vertical stress [MPa].

It is recommended to calculate vertical stress σ_z (unless the stress values measured using a tensor in situ are available) with the use of equation (2) stated in a paper by Carranza-Torres, Fairhurst (2000):

$$\sigma_z = 0.027 * z \quad (2)$$

where z is the depth at which the underground structure is located under the surface, in meters.

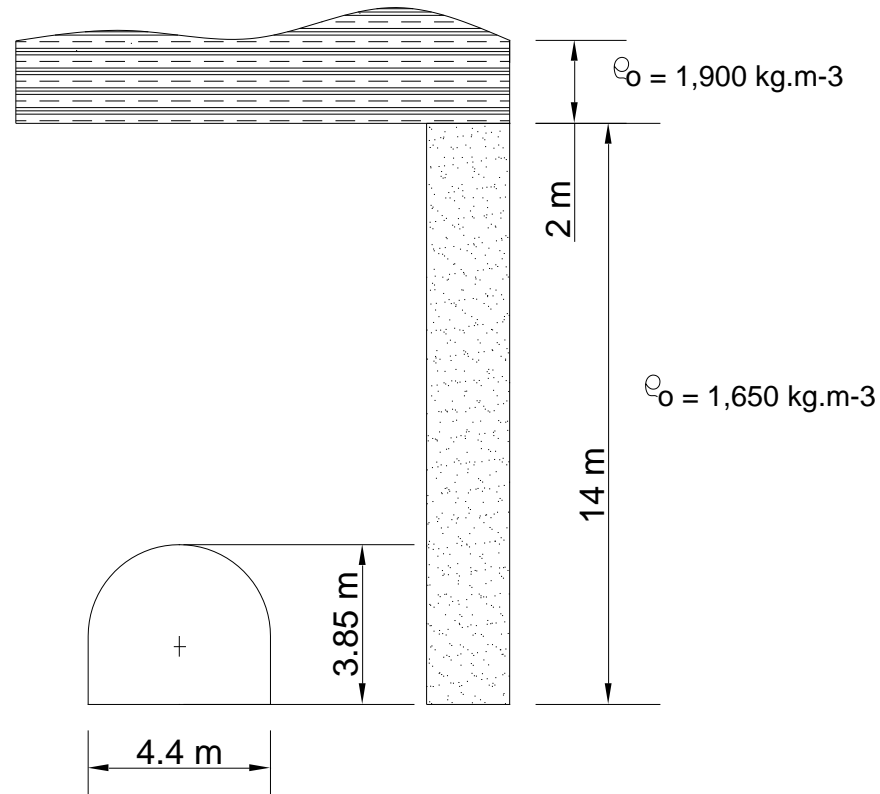


Fig. 16 Cross- section used for calculations

Equation (2) is based on the measurements of vertical stress in situ in various regions around the world, as modified by Hoek and Brown (1980) who hence created equation (2). Since the measurements in situ were carried out in rocks with an average unit weight $\gamma_o = 27 \text{ kN.m}^{-3}$ (Carranza-Torres, Fairhurst, 2000) and tuffite sands, which are dominating in the analysed area in terms of its thickness, exhibits a unit weight $\gamma_o \approx 17 \text{ kN.m}^{-3}$, vertical stress was calculated using a classical equation (3):

$$\sigma_z = \gamma_o * z \quad (3)$$

The unit weight of overburden rocks was calculated as a weighted arithmetic mean, and for the inputs shown in Fig. 16 the value of σ_z was 0.27 MPa, while $z = 16 \text{ m}$.

Horizontal stress σ_x was calculated using equation (4):

$$\sigma_x = k * \sigma_z \quad (4)$$

wherein k is the coefficient of lateral earth pressure, which may be calculated using equations created by various authors, such as:

$$k_a = \frac{1 - \sin \varphi}{1 + \sin \varphi} \quad (5)$$

$$k = \frac{\mu}{1 - \mu} \quad (6)$$

$$k = 5.13 * z^{-0.16} \quad (7)$$

wherein ϕ is the angle of friction of rocks or soils;

k_a – coefficient of active earth pressure, which was used due to the soil nature of tuffites; and

μ – Poisson's ratio of rocks or soils.

Tuffite sands have the character of overconsolidated sediments, therefore Jaky's formula for calculating the lateral pressure coefficient, which is recommended for normally consolidated soils (Boháč, J. et al., 2013), was not used.

Hoek and Brown (1980) modified the measurements of stress in situ into a graphical form, which contains the coefficients of lateral earth pressure observed in various regions of the world, delimited by two curves. The minimum value of the coefficient of lateral earth pressure was approximately $k \approx 0.5$ while the maximum value of horizontal stress was approximately a 3.5-fold of the average value of vertical stress. Results of in situ measurements indicated that in areas near the terrain surface, including the analysed area (Fig. 16), the coefficient of lateral earth pressure acquired values $k > 1$ (Carranza-Torres, Fairhurst, 2000).

A partial coefficient of the angle of friction of tuffites $\gamma_{\phi_r} = 1.21$ (Barták, J. et al., 2010) was used to calculate the angle of friction $\phi = 30^\circ$ (angle for tuffites $\phi = 36^\circ$, identified in the laboratory). With the calculated value of friction, the coefficient of lateral earth pressure was calculated using equation (5) with a resting value $k_a = 0.33$.

For tuffite sands, classified as class S1/S2 – clayey or silty sand, the value of the Poisson's ratio $\mu = 0.28$ was used as the benchmark. Using equation (6), the calculated coefficient value was $k = 0.39$ for value $\mu = 0.28$.

Using equation (7), created by Arjang (1998), the value of the coefficient of lateral earth pressure was calculated as $k = 3.3$ for the depth at which the testing room is located under the surface $z = 16$ m.

Depending on the equations used, the coefficient of lateral earth pressure acquired values falling within a wide range of values. Values k and k_a were used to calculate the average of lateral earth pressure $k = 3.3 + 0.33 + 0.39 / 3 \approx 1.3$, which was then used to calculate $\sigma_x = 1.3 * 0.27 \approx 0.35$ MPa. The reason for using the Arjang (1998) equation was the authors' effort to achieve a value of the average lateral

pressure coefficient that would approach the value $k \geq 1$, because in the authors' opinion this value is closer to the real behavior of the massif, i.e. the chimneying of the roof of corridors M1, M2 and M3 (Fig. 15) than the values $k \approx 0.3 - 0.4$, when the vertical stress is greater than the horizontal stress and failure should occur on the side walls of the underground works, which did not happen in reality. Brown and Hoek (1978) report the values $k = 2.54, 1.25, 1.23, 0.9$ for the lateral pressure coefficients measured in situ in tuff conditions, which approximately corresponds to the value $k = 1.3$ used in this article. The value of crack initiation stresses, as calculated using equation (1), was $\sigma_o = 0.31$ MPa.

Carranza-Torres and Fairhurst (2000) stated that if $k < k_{lim}$, then the CCM may also be applied to an uneven stress field in order to assess stability of underground structures, wherein k_{lim} is the limiting value of the coefficient of lateral earth pressure. The limiting coefficient k_{lim} was identified using the graph described in a paper by Carranza-Torres, Fairhurst (2000), while its values fell within the range $k_{lim} = <1.85-3>$ for the value of the angle of friction of tuffites $\phi = 30^\circ$. Since the lowest value $k_{lim} = 1.85 > 1.3$, the above stated requirement for the application of the CCM in a non-hydrostatic stress field was satisfied.

For a non-circular shape of the underground structure, an equivalent radius of the analysed structure R_{eq} was used, and the calculation was made using equation (8) (Kabwe, E. et al., 2019):

$$R_{eq} = \sqrt{\frac{A}{\pi}} \quad (8)$$

wherein A is the surface area of the analysed structure in m^2 .

For a transverse cross-section of the large tasting room with the height of the vertical wall $L = 1.65$ m (Fig. 16), the equivalent radius was $R_{eq} = 2.18$ m.

Critical reaction pressure of the support p_{cr} was calculated using equation (9):

$$p_{cr} = \sigma_o * (1 - \sin \varphi) - c * \cos \varphi \quad (9)$$

wherein c – cohesion of tuffites [MPa].

With the use of partial coefficient of tuffite cohesion $\gamma_{cr} = 1.25$ (Barták, J. et al., 2010), the calculated cohesion was $c = 24$ kPa (the cohesion value adopted from foreign literature was $c = 30$ kPa), (Asniar, N. et al., 2020).

Critical reaction pressure of the support p_{cr} corresponds to the critical value of displacement u_{cr} , which was calculated using equation (10):

$$u_{cr} = \frac{1 + \mu_t}{E_t} * \sigma_o * \left(1 - \frac{p_{cr}}{\sigma_o}\right) * R_{eq} \quad (10)$$

where μ_t - Poisson's ratio of tuffites [-]; and
 E_t - modulus of elasticity of tuffites [MPa].

Radius of the plastic zone R_p was calculated using equation (11):

$$R_p = R_{eq} \left[\frac{2}{(k_p + 1)} * \frac{(\sigma_o + c * ctg\varphi)}{(p_i + c * ctg\varphi)} \right]^{\frac{1}{k_p - 1}} \quad (11)$$

wherein p_i – fictitious support pressure [MPa], which fell within the interval $\langle p_{cr}, 0 \rangle$ in a selected step.

For a selected internal pressure of the support p_i , radial displacement of the excavated part u_r was calculated using equation (12):

$$u_r = \frac{1 + \mu_t}{E_t} * R_{eq} * \left[F_1 + F_2 * \left(\frac{R_{eq}}{R_p} \right)^{k_p - 1} + F_3 * \left(\frac{R_{eq}}{R_p} \right)^{k_{psi} + 1} \right] \quad (12)$$

wherein $k_p = \frac{1 + \sin \varphi}{1 - \sin \varphi}$, φ – friction angle, $k_{psi} = \frac{1 + \sin \psi}{1 - \sin \psi}$, ψ – dilation angle;

$$F_1 = -[(1 - 2 * \mu) * (\sigma_o + c * ctg\varphi)] ;$$

$$F_2 = \left[\frac{(1 - \mu) * (1 + k_p * k_{psi})}{(k_p + k_{psi})} - \mu \right] * \frac{2 * (\sigma_o + c * ctg\varphi)}{(k_p + 1)} ; \text{ and}$$

$$F_3 = \frac{2 * (1 - \mu) * (k_p - 1) * (\sigma_o + c * ctg\varphi)}{(k_p + k_{psi})}.$$

Deformation characteristics of the massif (GRC) located in the area of the large tasting room is shown in Fig. 18.

5.2 Deformation characteristics of the tuff support (SCC)

That curve represents the correlation between the reaction pressure of the tuff support and the displacement of the excavated part of the large tasting room. Deformation characteristics of the support may be expressed as a curve for various types of supports and combinations there of (sprayed concrete, bolts, steel support). It is calculated per unit length of the underground structure in its longitudinal axis.

Equations below, used for calculating deformation characteristics of the support, are provided in a paper by Carranza-Torres, Fairhurst (2000); the authors created them by modifying equations presented in papers by Hoek and Brown (1980) and Brady and Brown (1985).

If the stiffness of the tuff support is designated as K_t [MPa/m], the elastic region of the deformation characteristics of the support, i.e. the KR segment (Fig. 12), may be calculated using equation (13):

$$K_t = \frac{p_t}{u_r} \quad (13)$$

where p_t – load-bearing capacity of the tuff support [MPa],
 u_r – tuff support displacement [m].

The slope of the elastic region of the deformation characteristics of the support was calculated using equation (13) as a p_t/K_t ratio. The plastic region of the deformation characteristics of the support, i.e. the horizontal section beginning in point R, is determined by the maximum load-bearing capacity of the support p_t^{\max} before destruction (Fig. 12).

The maximum load-bearing capacity of the tuff support p_t^{\max} was calculated using equation (14):

$$p_t^{\max} = \frac{\sigma_t}{2} * \left[1 - \frac{(R_{eq} - t_t)^2}{R_{eq}^2} \right] \quad (14)$$

wherein σ_t – strength of the tuff support; and
 t_t – thickness of the tuff support [m].

Stiffness of the tuff support K_t was calculated using equation (15):

$$K_t = \frac{E_t}{(1 - \mu_t) * R_{eq}} * \frac{R_{eq}^2 - (R_{eq} - t_t)^2}{(1 - 2 * \mu_t) * R_{eq}^2 + (R_{eq} - t_t)^2} \quad (15)$$

where E_t – modulus of elasticity of the tuff support [MPa]; and
 μ_t – Poisson's ratio of the tuff support [-].

Equations (13) and (14) were derived for a circular shape of the support of the underground structure. For non-circular cross-sections, the analytical equations for calculating stiffness and maximum capacity of internal pressure of the support, which are necessary for the purpose of using the Convergence-Confinement Method, were not available.

Despite the simplification above (a circular versus non-circular cross-sections of the support), many authors, such as Russo and Repetto, 2009; Ascioğlu, G., 2007; Ayman, A., M., et al., 2009; Rahmannedjad, R. et al., 2015; Sebbeh-Newton, S. et al., 2021; etc. applied the CCM to their assessment of stability of underground structures with a non-circular cross-section.

An assessment of stability of non-circular cross-sections of underground structures may also be carried out by applying not only numerical modelling, but also procedures used in the conventional statics of buildings dating back to the last century, as described by many authors, e.g. Kommerell (1912), Bierbaumer (1913), Zurabov and Bugajevova in Szechy, K. (1967), or by applying the hyperstatic reaction method (Oreste, 2007).

A planar support with a circular shape in a hydrostatic stress field is exposed to compressive stresses without the formation of internal forces (bending moments, normal forces, shear forces) in a radial cross-section; therefore, when calculating p_t^{\max} using equation (13), the uniaxial compressive strength of sprayed or pumped concrete of various ages (e.g. 1-, 5-, 10-, or 28-day-old compressive strength etc.) was used as the allowable stress of the support.

With a non-circular cross-section, a certain part, for example, the arch section of the tuff support, may be loaded by the loosening layers of tuffites, which induce bending (flexural) tensile stresses that affect the weight-carrying cross-section. Under the tensile bending stress, the external part of the loaded cross-section is exposed to compressive stress while the internal part of the cross-section is exposed to tensile stress.

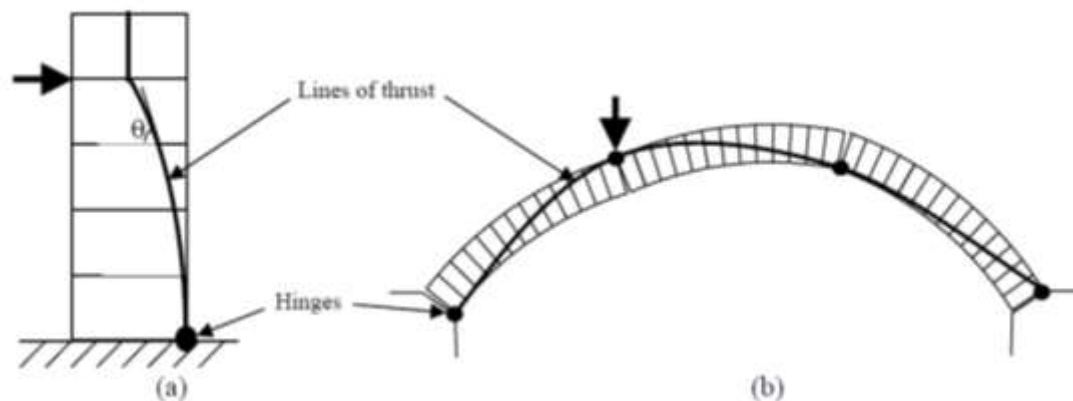


Fig. 17 Thrust line at a collapse (a) of the support and (b) of the arch (Gilbert, M., 2007)

Above the place of the point load, the external side is exposed to thrust while the internal side is exposed to tensile force. Outside of the area of the point load, the deterioration process is the opposite (Fig. 17).

Vertical parts of the cross-section used for calculations may be exposed to tensile as well as compressive stresses. Similarly, the arch part of the cross-section may be exposed to thrust or tensile force, primarily depending on the magnitude and direction of the exerted crack initiation stresses in the rock massif.

Combined stresses to which the support cross-section is exposed may be assessed by applying numerical modelling; nevertheless, the application of those methods to conditions with an uneven, non-constant thickness of the tuff cladding also has certain limitations.

Due to the facts stated above, with an allowable stress of the tuff support σ_t , the calculation of p_t^{\max} , which was made using equation (13), was based on uniaxial compressive strength, transverse tensile strength of tuff, and flexural tensile strength.

According to the STN 731101 standard titled Masonry Structures of 1989, the material reliability coefficient $\gamma_m = 2$ should be used for excessively damp walls when calculating an allowable stress of a wall.

Allowable stress of the tuff support at uniaxial compressive pressure σ_{ctd} was calculated using equation (16):

$$\sigma_{ctd} = \frac{\sigma_{ct}}{\gamma_m} = \frac{4.7}{2} = 2.35 \text{ MPa} \quad (16)$$

wherein σ_{ct} – uniaxial compressive strength of wet tuff, identified in the laboratory [MPa].

Allowable stress of the tuff support at transverse tensile stress σ_{ttd} was calculated using equation (17):

$$\sigma_{ttd} = \frac{\sigma_{tt}}{\gamma_m} = \frac{0.8}{2} = 0.4 \text{ MPa} \quad (17)$$

wherein σ_{tt} is the transverse tensile strength of wet tuff, identified in the laboratory [MPa].

Allowable tensile bending stress of the tuff support σ_{ftd} was calculated using equation (18):

$$\sigma_{ftd} = \frac{\sigma_{ft}}{\gamma_m} = \frac{1.4}{2} = 0.7 \text{ MPa} \quad (18)$$

wherein σ_{ft} is the flexural (bending) strength of wet tuff, identified in the laboratory [MPa].

The calculation of deformation characteristics of the tuff support in the large tasting room was made using a thickness $t_t = 0.25$ m. Equation (13) was used to calculate the maximum load-bearing capacity of the tuff support p_t^{\max} for 3 different values of allowable stress of the tuff support using equations (16), (17) and (18), which were subsequently used to construct the deformation characteristics of the tuff support.

Similarly to the calculations made using equations (16), (17) and (18), the modulus of elasticity of the tuff support E_t was calculated as the quotient of the modulus of elasticity identified in the laboratory in the wet state and the material reliability coefficient, calculated with the use of equation (19):

$$E_t = \frac{E_{tl}}{\gamma_m} = \frac{1,208}{2} = 604 \text{ MPa} \quad (19)$$

wherein E_{tl} – modulus of elasticity of wet tuff, identified in the laboratory [MPa].

In the calculation of stiffness of the tuff support K_t , made using equation (15), the following deformation properties of the tuff support were used:

The modulus of elasticity – $E_t = 604$ MPa; and

The Poisson's ratio – $\mu_t = 0.43$.

5.3 Longitudinal deformation profile (LDP) of the large tasting room

An important part of the Convergence-Confinement Method is also the calculation of the deformation profile of the underground structure in its longitudinal axis. It provides information on how quickly an interaction between the rock massif and the support behind the working face of the excavated structure occurs.

Based on the known values of radial displacement in the longitudinal axis of the large tasting room before and behind its working face, it is possible to calculate the crack opening displacement u_{in} that occurred before the permanent tuff support was built (Fig. 12).

According to Paneta (1995), crack opening displacement u_{in} [m] may be calculated using equation (20):

$$u_{in} = \lambda * u_{el} \quad (20)$$

$$\text{wherein } \lambda = 0.25 + 0.75 * \left[1 - \left(\frac{0.75 * R_{eq}}{0.75 * R_{eq} + x} \right)^2 \right]$$

wherein x is the advance distance of the working face before the place of construction of the tuff support [m].

Elastic displacement u_{el} is the maximum elastic displacement calculated at zero resistance pressure of the support, i.e. when the tasting room is without the support, using equation (21):

$$u_{el} = \frac{1 + \mu}{E} * \sigma_o * R_{eq} \quad (21)$$

The tuff support in the large testing room was not built after each partial excavation, but after a certain time period after a relevant part of the working face was made; therefore, the advance distance of the working face was determined as $x = 10$ m. The value of crack initiation stress in the massif was determined as $\sigma_o = 0.31$ MPa, as stated in Subchapter 5.1.

In the validation of stability of the large tasting room by applying the CCM, the following input parameters were used:

Rock massif – tuffites

$E = 100$ MPa

$\mu = 0.28$

$$\text{coh} = 24 \text{ kPa}$$

$$\phi = 30^\circ$$

$$\psi = 0^\circ$$

$$\gamma_o = 16.81 \text{ kN.m}^{-3}$$

$$\sigma_o = 0.31 \text{ MPa}$$

Large testing room

$$R_{\text{eq}} = 2.18 \text{ m}$$

$$x = 10 \text{ m}$$

Tuff support

$$E_t = 604 \text{ MPa}$$

$$\mu_t = 0.43$$

$$t_t = 0.25 \text{ m}$$

$$\sigma_t = 2.35 \text{ MPa}; 0.4 \text{ MPa}; 0.7 \text{ MPa}$$

The assessment of stability of the large tasting room with the input parameters above is graphically depicted in Fig. 18.

5.4 Deformation characteristics of the large tasting room for loaded terrain surface

This Subchapter presents the constructed deformation characteristics of the massif in the cross-section leading through the large tasting room with the terrain surface exposed to an evenly distributed load q , which will be exerted by the planned construction of a new residential complex above a part of the existing wine cellars, the so-called original wine cellars (Fig. 13).

The evenly distributed load of the terrain surface q was taken into account in the GRC calculation with the use of a fictitious height h' , which was calculated using equation (22):

$$h' = \frac{q}{\gamma_o} = \frac{50}{16.81} \approx 3 \text{ m} \quad (22)$$

wherein q is the evenly distributed load exerted on the terrain surface [kN.m^{-2}]; and
 γ_o – unit weight of overburden rocks or soils [kN.m^{-3}].

The fictitious height h' was added to the original height z , which represents the height of the overburden layer and the height of the large tasting room (Fig. 16).

The most important results of the Convergence-Confinement Method, which was applied to the assessment of stability of the large tasting room that was excavated in tuffites and secured with a tuff support, are shown in Fig. 18.

Deformation characteristics of the massif present in the profile of the large tasting room with the maximum radial displacement $u_r^{\max} = 0.0261$ m was calculated and constructed for the input parameters presented at the end of Subchapter 5.3.

Under a planar load of the terrain surface $q = 50$ kPa, there was a change in the course of deformation characteristics; in particular, there was a shift upwards compared to the baseline GRC, while the maximum radial displacement was $u_{rq}^{\max} = 0.0346$ m.

Deformation characteristics of the support were constructed for 3 different values of allowable stress $\sigma_t = 0.4$ MPa; 0.7 MPa; and 2.35 MPa, for which the maximum load-bearing capacity was calculated: $p_s^{\max1} = 0.043$ MPa; $p_s^{\max2} = 0.076$ MPa; and $p_s^{\max3} = 0.254$ MPa for the selected parameters of the support (see equation 14) (Fig. 18, points 1, 2, and 3).

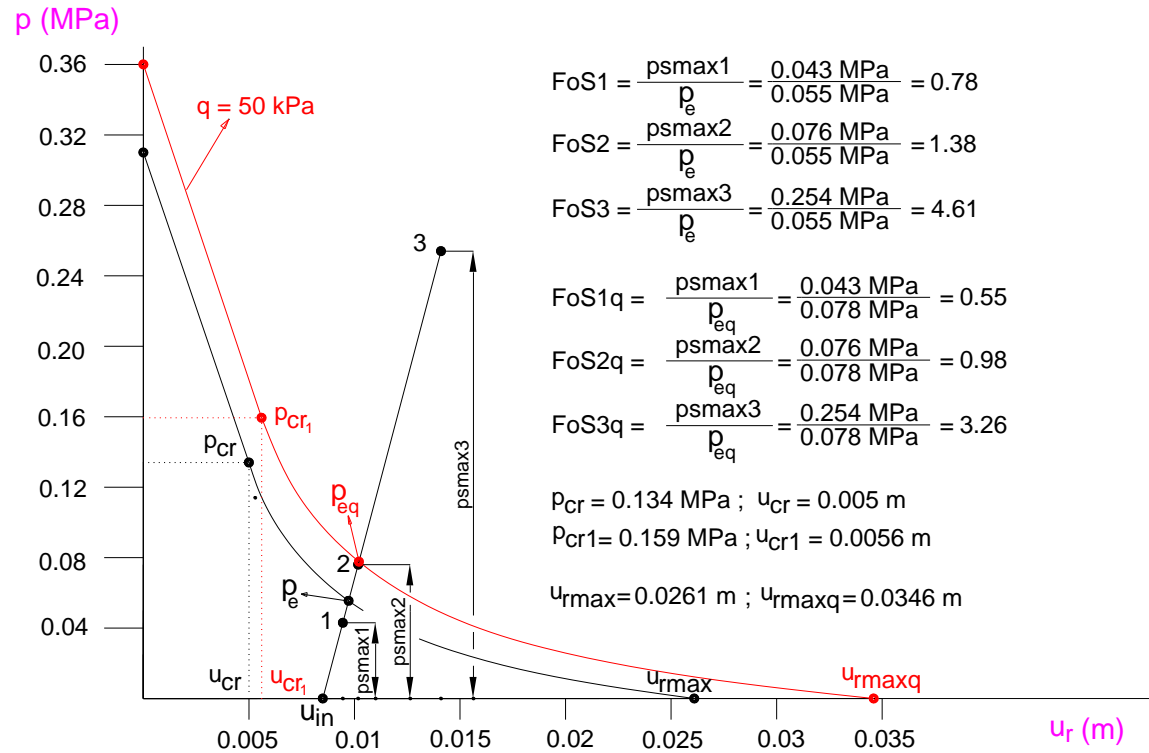


Fig. 18 CCM results – large testing room

If there is no intersection in the GRC/SCC system, then $FoS < 1$ and the rock-support system is imbalanced. Fig. 18 shows such a state, occurring at GRC without exposure to a surface load, provided that transverse tensile strength σ_{ttd} of the tuff is used at the allowable stress of the support (point 1 in Fig. 18), or if transverse tensile strength σ_{ttd} and flexural bending strength σ_{ftd} are used at the allowable stress at GRC with exposure to surface load (point 2 in Fig. 18).

Factor of safety $FoS > 1$ if there is an intersection in the GRC/SCC system and the rock-support system is balanced; in Fig. 18, the corresponding points are p_e and p_{eq} . In the case that allowable stress of the support is replaced with uniaxial compressive strength of tuff σ_{ctd} , then the following applies to GRC with and without exposure to evenly distributed load q : $FoS > 1$. If allowable stress is replaced with flexural bending strength σ_{ftd} , then $FoS > 1$ also in the case of GRC without exposure to surface load q .

Concrete values of FoS for the individual combinations of allowable stress of the tuff support and deformation of the excavated part of the large tasting room in tuffites are shown in Fig. 18.

6. Conclusion

Despite certain simplifications, the CCM is still used at present, especially in the process of preliminary designing of primary tunnel linings made of sprayed concrete, as well as in assessment of stability of underground structures of other types.

The advantage of the CCM is that it is fast and flexible, when compared to numerical modelling, in particular 3D modelling, which facilitates conducting a wide range of parametric studies for those of the parameters the values of which are not fully reliable (e.g. properties of the massif, properties of the brick-laid support, crack initiation stresses, etc.).

In the conducted validation of stability of the underground structure, which was of relatively large transverse dimensions (the large tasting room), secured with a brick-laid tuff support, located in the Tokaj Wine Region in the Slovak Republic, the CCM confirmed good concordance between the results of the numerical and analytical approaches.

Stability of the large tasting room was unchanged in the cases without exposure to additional planar load of the terrain, except for the cases in which the uniaxial tensile force is formed in the tuff support.

Evenly distributed load exerted by the terrain surface will cause considerable deterioration of stability of the large tasting room. Stability of tuff cellars with a different height of the overburden layer and different transverse cross-sections may be assessed in a similar manner, as described above.

Acknowledgements

This research was supported by projects VEGA 2/0090/23 and APVV-23-0364.

References:

- ARJANG, B. (1998): Canadian crustal stresses and their application to mine design. *Mine planning and equipment selection*. Balkema, Rotterdam, pp. 269-274.
- ASCIOGLU, G. (2007): Analysis of support design practice at Elmalik Portals of Bolu tunnel. In partial fulfillment of the requirements for the degree of Master of Science in Mining Engineering. Ms. Sc. Aralik.

- ASNIAR, N., PURWANA, N.Y., SURJANDARI, N.S (2019): Tuffs as rock and soil: Review of the literature on tuff geotechnical, chemical and mineralogical properties around the world and in Indonesia. *AIP Conference Proceedings*. pp. 050022-1–050022-9.
- AYMAN, A.M., BELAL, M.A., EL-DESOUKY, A. (2009): Application of the Convergence-Confinement Approach to Analyze the Rock-Lining Interaction in Tunnels (Case Study: Shimizu Tunnel). *13th International Conference On AEROSPACE SCIENCES & AVIATION TECHNOLOGY, ASAT- 13*, Egypt, May 26 – 28, pp. 1/1 – 1/11.
- BAŇACKÝ, J., ELEČKO, M., KALIČIAK, M., LEXA, J., STRAKA, P., VASS, D., VOZÁR, J., VOZÁROVÁ, A. (1988): *Geologická mapa južnej časti Východoslovenskej nížiny a Zemplínskych vrchov*. Vydavateľstvo D. Štúra, ŠGÚDŠ, Bratislava.
- BARTAK, J. et al.. (2010): *Doporučení pro zpracování statických výpočtu ražených tunelu dle EC*. Praha.
- BIERBAUMER, A. (1913): *Die Dimensionierung des Tunnelmauerwerkes*. Leipzig.
- BRADY, B.G.H., BROWN, E.T. (1985): *Rock Mechanics for Underground Mining* (Second ed.). New York: Chapman & Hall.
- BOHÁČ, J., MAŠÍN, D., MALÁT, R., NOVÁK, V., ROTT, J. (2013): Methods of determination of K_0 in overconsolidated clay. *Proceedings of the 18th International Conference on Soil Mechanics and Geotechnical Engineering, Paris 2013*: pp. 203 – 206.
- BROWN, E.T., HOEK, E. (1978): Trends in Relationships between Measured in-Situ Stresses and Depth. *Int. J. Rock Mech. Min. Sci. & Geomech. Abstr.* Vol. 15, pp. 211-215. 0020-7624/78/0801-0211502.00/0 © Pergamon Press Ltd 1978. Printed in Great Britain.
- BROWN, E.T., BRAY, W., LADANYI, B., HOEK, E. (1983): Ground Response Curves for Rock Tunnels - *Journal of Geotechnical Engineering* 109: pp. 15- 39.
- CARRANZA-TORRES, C. (2003): Dimensionless graphical representation of the exact elastoplastic solution of a circular tunnel in a Mohr-Coulomb material subject to uniform far-field stresses. *Rock Mech Rock Eng*; 36(3), pp. 237–253.
- CARRANZA-TORRES, C., FAIRHURST, C. (1999): The elasto-plastic response of underground excavations in rock masses that satisfy the Hoek-Brown failure criterion. *Int. J. Rock&Mech Min Sci*; 36(6): pp. 777–809.
- CARRANZA-TORRES, C., FAIRHURST, C. (2000): Application of the Convergence-Confinement Method of Tunnel Design to Rock Masses That Satisfy the Hoek-Brown Failure Criterion. *Tunnelling and Underground Space Technology*, Vol. 15, No. 2, pp. 187-213.
- CONTRERAS, A.C., DE CABO, M., FERNÁNDEZ, E., GALERA, J.M., MEYER, P. (2008): The construction of the San Cristóbal tunnel (Santiago de Chile). In: *ITA-AITES World Tunnel Congress, Agra/India*, pp.832-847.
- COVASSI, P., ZEBALLOS, M., GOROSITO, S. (2015): Geotechnical Characterization of a Pyroclastic Sand and Tuff. Conference Paper November 2015. *Deformation Characteristics of Geomaterials* V.A. Rinaldi et al. (Eds.)IOS Press, pp.1121-1128.
DOI: [10.3233/978-1-61499-601-9-1121](https://doi.org/10.3233/978-1-61499-601-9-1121).
- DUNCAN FAMA, M. E. (1993): Numerical Modeling of Yield Zones in Weak Rock. In *Comprehensive Rock Engineering*, (ed. J.A. Hudson) 2. Oxford: Pergamon, pp. 49-75.
- FEDER, G., ARWANITAKIS, M. (1977): Zur Gebirgsmechanik ausbruchsnaher Bereiche tiefliegender Hohlrumbaute. *Berg und Huettenmaennische Monatshefte*.
- FENNER, R. (1938): Untersuchungen zur Erkenntnis des Gebirgsdrucks. *Glückauf* 74, pp. 681-695 and 705-715.

- GILBERT, M. (2007): Limit analysis applied to masonry arch bridges: state-of-the-art and recent developments. Proceedings of 5th International Conference on Arch Bridges (ARCH'07), PB Lourenço, DB Oliveira, and A. Portela, eds., Funchal, Madeira, Portugal, pp. 13 – 28.
- GIRMSCHIED, G. (2008): *Baubetrieb und Bauverfahren im Tunnelbau*. 2. Auflage, Ernst & Sohn A Wiley Company, Berlin.
- HOEK, E. (1990): Estimating Mohr-Coulomb friction and cohesion values from the Hoek-Brown failure criterion. *Int. J. Rock Mech. Min. Sci. & Geomech. Abstr.* 27 (3), pp. 227-229.
- HOEK, E. (1998): Tunnel support in weak rock. Proc. Regional Symp. on Sedimentary Rock Engineering, Taipei, Taiwan, Nov 20-22, pp. 1-12.
- HOEK, E. (1999): Support for very weak rock associated with faults and shear zones. Proc. International Symposium on Rock Support and Reinforcement Practice in Mining, Kalgoorlie, Australia, 14-19 March, pp. 1 – 20.
- HOEK, E., BROWN, E.T. (1980): *Underground Excavations in Rock*. London: The Institute of Mining and Metallurgy. 527 p.
- HOEK, E., BROWN, E.T. (1997): Practical estimates of rock mass strength. *Int. J. Rock Mech. Min. Sci. & Geomech. Abstr.* 34 (8), pp. 1165-1186.
- ISRM: Suggested Methods published between 1974 and 2006.
- KABWE, E., KARAKUS, M., CHANDA, E. (2019): Proposed solution for the ground reaction of non-circular tunnels in an elastic-perfectly plastic rock mass - *ScienceDirect. Computers and Geotechnics* 119, pp. 1 – 15.
<https://doi.org/10.1016/j.compgeo.2019.103354>.
- KASTNER, H. (1971): *Statik des Tunnel-und Stollenbaus auf der Grundlage geomechanischer Erkenntnisse*. Zweite Neubearbeitete Auflage.
- KOMMERELL, O. (1912): *Statische Berechnung des Tunnelmauerwerkes*. Berlin.
- KLEPSATEL, F., MAŘÍK, L., FRANKOVSKÝ, M. (2005): *Městské podzemní stavby*. Jaga, Bratislava.
- LEE, Y-K., PIETRUSZCZAK, S. (2014): A new numerical procedure for elasto-plastic analysis of a circular opening excavated in a strain-softening rock mass. *Tunnelling and Underground Space Technology*, Vol. 23, No. 5, pp. 588-599.
- LIU, N., HUANG, Y-X., CAI, W., CHEN, K. (2020): Application of Improved Single-Hole Superposition Theory in Nonequal Cross-Section Tunnel Intersection. *Hindawi Advances in Civil Engineering* Volume 2020, Article ID 8837480, 15 pages.
<https://doi.org/10.1155/2020/8837480>.
- MAZÚR, E., LUKNIŠ, M. (1986): Geomorfologické členenie SSR a ČSSR. Časť Slovensko. Atlas Slovenskej socialistickej republiky, Slovenská kartografia Bratislava.
- ORESTE, P.P., PEILA, D. (1997): Modelling Progressive Hardening of Shotcrete in Convergence-Confinement Approach to Tunnel Design. *Tunnelling and Underground Space Technology*, Vol. 12, No. 3, pp. 425—431.
- ORESTE, P. P. (2007): A numerical approach to the hyperstatic reaction method for the dimensioning of tunnel supports. *Tunnelling and Underground Space Technology* 22, pp. 185–205.

doi:10.1016/j.tust.2006.05.002

- PACHER, F. (1964): Deformations Messungen in Versuchstollen als Mittel zur Erforschung des Gebirgsverhaltens und zur Bemessung des Ausbaues. *Felsmechanik und Ingenieursgeologie*, Supplementum IV/1964.
- PANET, M. (1995): *Le calcul des tunnels par la méthode convergence confinement*. - Paris, Presses de l'ENPC: 177.
- PANET, M., GUENOT, A. (1983): Analysis of convergence behind the face of a tunnel. *Tunnelling* 82, proc. of the 3rd international symposium - Brighton, 7-11 June 1982 - London: pp. 197-204.
- RAHMANNEJAD, R., KARGAR, A.R., MAAZALLAHI, V., GHOTBI-RAVANDI, E. (2015): Analytical analysis of ultimate ground pressure on tunnel support system. *Journal of Mining & Environment*, Vol.6, No.2, pp. 151-157.
- RATKOVSKÝ, K., KLEPSATEL, F. (1980): *Podzemné stavby I*. Stavebná Fakulta SVŠT Bratislava.
- RUSSO, G., REPETTO, L., PIRAUD, J., R. LAVIGUERIE, R. (2009): Back-analysis of the extreme squeezing conditions in the exploratory adit to the Lyon-Turin base tunnel. ROCKENG09: Proceedings of the 3rd CANUS Rock Mechanics Symposium, Toronto, May 2009 (Ed: M.Diederichs and G. Grasselli), paper 4127 -1/13.
- SALENCON, J. (1969): Contraction quasi-statique d'une cavité à symétrie sphérique ou cylindrique dans un milieu elastoplastique. *Annales des ponts et chaussées*, Vol. 4., pp. 231–236.
- SANTOLO, A.S., EVANGELISTA, L., SILVETRI, F., CAVUOTO, G., FIORE, V., PUNZO, M., TARALLO, D., EVANGELISTA, A. (2015): Investigations on the stability conditions of a tuff cavity: the Cimitero delle Fontanelle in Naples. *RIVISTA ITALIANA DI GEOTECNICA*, 3, pp. 28 - 46.
- SEBBEH_NEWTON, S., SHEHU, A.S.H., AYWAH, P., KABA, A.A., ZABID, H. (2021): Analytical and numerical assessment of a preliminary support design – a case study. *Cogent Engineering*, 8: 1869367, pp. 1 – 20. <https://doi.org/10.1080/23311916.2020>
- STN 73 1101 *Murované konštrukcie*, 1989.
- SZECHY, K. (1967): *The Art of Tunneling*. Akadémiai Kiadó, Budapest.
- VARGA, M. (2012): *Veľká Bara – Borex*. Záverečná správa. Orientačný inžinierskogeologický prieskum. MontanA, s.r.o. Košice, 2012.
- VARGA, M. (2012): *Veľká Bara – Borex*. Záverečná správa. Doplnkový inžinierskogeologický prieskum. MontanA, s.r.o. Košice, 2012.
- VLACHOPOULOS, N., DIEDERICHS, M.S. (2009): Improved longitudinal displacement profiles for convergence-confinement analysis of deep tunnels. *Rock Mechanics and Rock Engineering* 42, pp. 131 – 146.
doi: 10.1007/s00603-009-0176-4
- VLACHOPOULOS, N., DIEDERICHS, M.S. (2014): Appropriate Uses and Practical Limitations of 2D Numerical Analysis of Tunnels and Tunnel Support Response. *Geotech Geol Eng* 32: pp. 469–488.
doi: 10.1007/s10706-014-9727-x
- ŽEC, B., VARGOVÁ, V. (2010): *Veľká Bara – Borex*. Záverečná správa. Orientačný inžinierskogeologický prieskum. Geoslovakia Košice.

Authors:

¹Ing. Pavol Vavrek, PhD. – Institute of Geotechnics SAS, Watsonova 45, 040 01 Kosice, Slovakia

vavrek@saske.sk

²Ing. Edita Lazarová, PhD. – Institute of Geotechnics SAS, Watsonova 45, 040 01 Kosice, Slovakia

lazarova@saske.sk

³Ing. Mária Bali Hudáková, PhD. – Institute of Geotechnics SAS, Watsonova 45, 040 01 Kosice, Slovakia

krulakova@saske.sk

⁴Ing. Alexander Kiovský – Institute of Geotechnics SAS, Watsonova 45, 040 01 Kosice, Slovakia

kiovsky@saske.sk

⁵Ing. Vít'azoslav Krúpa, DrSc. – Institute of Geotechnics SAS, Watsonova 45, 040 01 Kosice, Slovakia

krupa@saske.sk

⁶Ing. Lucia Ivaničová, PhD. – Institute of Geotechnics SAS, Watsonova 45, 040 01 Kosice, Slovakia

ivanic@saske.sk